

Cardiac-type EC-Coupling in Dysgenic Myotubes Restored with Ca^{2+} Channel Subunit Isoforms α_{1C} and α_{1D} Does not Correlate with Current Density

Nicole Kasielke,* Gerald J. Obermair,[†] Gerlinde Kugler,* Manfred Grabner,* and Bernhard E. Flucher*[†]

*Department of Biochemical Pharmacology and [†]Department of Physiology, University of Innsbruck, A-6020 Innsbruck, Austria

ABSTRACT Ca^{2+} -induced Ca^{2+} -release (CICR)—the mechanism of cardiac excitation-contraction (EC) coupling—also contributes to skeletal muscle contraction; however, its properties are still poorly understood. CICR in skeletal muscle can be induced independently of direct, calcium-independent activation of sarcoplasmic reticulum Ca^{2+} release, by reconstituting dysgenic myotubes with the cardiac Ca^{2+} channel α_{1C} ($\text{Ca}_v1.2$) subunit. Ca^{2+} influx through α_{1C} provides the trigger for opening the sarcoplasmic reticulum Ca^{2+} release channels. Here we show that also the Ca^{2+} channel α_{1D} isoform ($\text{Ca}_v1.3$) can restore cardiac-type EC-coupling. GFP- α_{1D} expressed in dysgenic myotubes is correctly targeted into the triad junctions and generates action potential-induced Ca^{2+} transients with the same efficiency as GFP- α_{1C} despite threefold smaller Ca^{2+} currents. In contrast, GFP- α_{1A} , which generates large currents but is not targeted into triads, rarely restores action potential-induced Ca^{2+} transients. Thus, cardiac-type EC-coupling in skeletal myotubes depends primarily on the correct targeting of the voltage-gated Ca^{2+} channels and less on their current size. Combined patch-clamp/fluo-4 Ca^{2+} recordings revealed that the induction of Ca^{2+} transients and their maximal amplitudes are independent of the different current densities of GFP- α_{1C} and GFP- α_{1D} . These properties of cardiac-type EC-coupling in dysgenic myotubes are consistent with a CICR mechanism under the control of local Ca^{2+} gradients in the triad junctions.

INTRODUCTION

Excitation-contraction (EC) coupling in muscle depends on the close interaction of a voltage-gated Ca^{2+} channel in the t-tubule or the plasma membrane with a Ca^{2+} release channel (ryanodine receptor, RyR) in the sarcoplasmic reticulum (SR). In cardiac EC-coupling this interaction is mediated by Ca^{2+} entering the cell through a voltage-gated Ca^{2+} channel that in turn activates Ca^{2+} release from the SR. In skeletal muscle, SR Ca^{2+} release is activated in the absence of Ca^{2+} influx, presumably by a physical interaction of the two Ca^{2+} channels. Under experimental conditions, the skeletal muscle Ca^{2+} release channel (RyR1) can also be activated by μM concentrations of cytoplasmic free Ca^{2+} (Nagasaki and Kasai, 1983; Smith et al., 1986). Whether Ca^{2+} -induced Ca^{2+} -release (CICR) in skeletal muscle occurs under physiological conditions, and if so, to what extent it contributes to skeletal muscle EC-coupling is still not resolved.

Reconstitution of Ca^{2+} channel null-mutant skeletal myotubes with wild-type and mutant heterologous Ca^{2+} channels has been a potent tool for analyzing the mechanism of EC-coupling in an intact muscle system. Normal function can be restored in dysgenic myotubes, which lack the skeletal muscle Ca^{2+} channel α_{1S} subunit, by heterologous expression of α_{1S} (Tanabe et al., 1988). When dysgenic myotubes are reconstituted with the cardiac Ca^{2+} channel α_{1C} subunit,

“cardiac-type” EC-coupling is restored, which is characterized by its dependence on Ca^{2+} influx (Tanabe et al., 1990). Presumably the skeletal muscle Ca^{2+} release channel is activated by trigger Ca^{2+} entering the myotube through α_{1C} . However, not all examined Ca^{2+} channel isoforms that produced Ca^{2+} currents when expressed in dysgenic myotubes also triggered CICR from the SR. The neuronal isoform α_{1A} , which is not targeted into triads of dysgenic myotubes, only very rarely displayed evoked contractions (Adams et al., 1994) or Ca^{2+} transients in response to electrically induced action potentials (action potential-induced Ca^{2+} transients) (Flucher et al., 2000). Apparently the correct subcellular distribution of the channel is important for the activation of cardiac-type EC-coupling in skeletal myotubes. Skeletal-type EC-coupling properties could be conferred onto the cardiac α_{1C} subunit by replacing a short sequence of the cytoplasmic loop connecting the homologous repeats II and III with that of α_{1S} (Nakai et al., 1998). Thus, the chimera CSk53 was created, which combines skeletal-type activation of EC-coupling with cardiac current properties.

If CICR participates in normal skeletal muscle EC-coupling, it is unlikely that the trigger Ca^{2+} comes from the Ca^{2+} currents across the sarcolemma, because the slow activation of the skeletal Ca^{2+} current lags behind activation of SR calcium release (Garcia et al., 1989; Feldmeyer et al., 1990). Instead, trigger Ca^{2+} must be provided by Ca^{2+} released from the SR by the population of the skeletal muscle RyR1 that is under the direct control of the voltage-sensor α_{1S} subunit (reviewed in Rios and Stern, 1997). In other words, Ca^{2+} released through the RyR1 provides a positive feedback resulting in release of more Ca^{2+} from the same or adjacent RyRs. A recent report by O'Brien et al. (2002) indicates that, whereas CICR appears not to be necessary for

Submitted December 6, 2002, and accepted for publication February 7, 2003.

Address reprint requests to Dr. Bernhard E. Flucher, Dept. of Physiology, University of Innsbruck, Fritz-Pregl-Str. 3, A-6020 Innsbruck, Austria. Tel.: +43-512-507-3787; Fax: +43-512-507-2836; E-mail: bernhard.e.flucher@uibk.ac.at.

© 2003 by the Biophysical Society

0006-3495/03/06/3816/13 \$2.00

activation of EC-coupling in skeletal muscle, SR Ca^{2+} release is reduced by fivefold when Ca^{2+} activation of RyR1 is impeded. This indicates a significant contribution of CICR to skeletal muscle EC-coupling.

Here we studied the properties of CICR in skeletal myotubes separate from skeletal-type activation of Ca^{2+} release by expressing nonskeletal α_1 subunits with distinct current characteristics and with distinct targeting characteristics in dysgenic myotubes. Analyzing the capability of different types of Ca^{2+} channels to generate action potential-induced and voltage-clamp-induced Ca^{2+} transients indicates that in the absence of direct skeletal coupling, Ca^{2+} currents of similar size as those of the skeletal α_{1S} are sufficient to trigger CICR. Moreover, the results indicate that activation of SR Ca^{2+} release seems to depend less on the magnitude of the whole-cell current than on the correct localization of the channels in the triads.

MATERIALS AND METHODS

Cell culture and transfections

Myotubes of the homozygous dysgenic (*mdg/mdg*) cell line GLT were cultured as described in Powell et al. (1996). At the onset of myoblast fusion (2 days after addition of differentiation medium), GLT cultures were transfected using FuGene transfection reagent (Roche, Basel, Switzerland). Cultures were analyzed 3–5 days after transfection.

α_1 subunit constructs

The following GFP-tagged Ca^{2+} channel constructs have been used: α_{1S} , α_{1A} , α_{1C} (Grabner et al., 1998), α_{1D} (Koschak et al., 2001), and α_{1G} (Monteil et al., 2000). GFP-CSk53: The *Bam*HI-*Eco*RV fragment (nt 1265–4351; α_{1C} numbering) of clone CSk53 (Nakai et al., 1998), where part of the II-III loop coding α_{1C} cDNA sequence (nt 2549–2690) was replaced by α_{1S} sequence (nt 2156–2297), was ligated into the corresponding restriction enzyme sites of clone GFP- α_{1C} (Grabner et al., 1998) resulting in an N-terminally GFP-tagged CSk53.

GFP and immunofluorescence labeling

Differentiated GLT cultures were fixed and immunostained as previously described (Flucher et al., 1994; Flucher et al., 2000). For double-immunofluorescence labeling we used an affinity-purified anti-GFP antibody (Molecular Probes, Eugene, OR) at a final dilution of 1:4000 and the affinity-purified antibody 162 (Giannini et al., 1995) against RyR1 at a dilution of 1:5000. Alexa-488- and Alexa-594-conjugated secondary antibodies (Molecular Probes) at dilutions of 1:4000 were used to achieve a wide separation of the fluorescence signals. Alexa-488 was usually used with the anti-GFP antibody so that the antibody label and the intrinsic GFP signal were both recorded in the green channel. Controls, for example multiple combinations of primary and secondary antibodies and the omission of primary antibodies, were routinely performed.

Images of the double labeling experiments were recorded on an Axiophot microscope (Carl Zeiss, Jena, Germany) using a cooled CCD camera and Meta View image processing software (Universal Imaging Corporation, West Chester, PA). Quantitative analysis of the labeling patterns was performed by systematically screening the cover glasses for transfected myotubes using a 63 \times objective. The labeling pattern in transfected myotubes with more than two nuclei was classified as “clustered” when

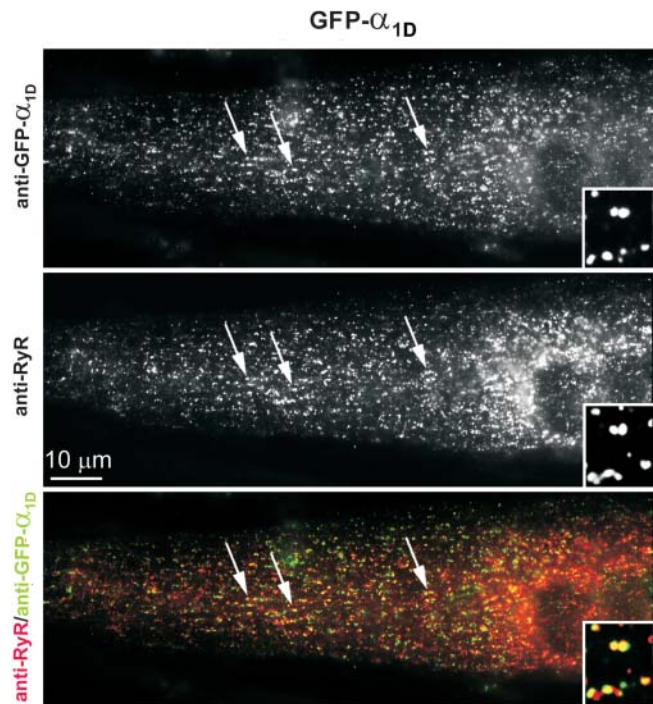


FIGURE 1 The L-type Ca^{2+} channel subunit GFP- α_{1D} is targeted into skeletal muscle triads of dysgenic myotubes. Dysgenic myotubes transfected with GFP- α_{1D} were double immunofluorescence labeled with antibodies against GFP (*top*) and against the skeletal muscle RyR1 (*middle*). GFP- α_{1D} is distributed in clusters co-localized with RyR1 (examples indicated by arrows), which indicates a localization of GFP- α_{1D} in junctions of the SR with the plasma membrane or the t-tubules (triads). The color overlay (*bottom*) shows the co-localization of GFP- α_{1D} clusters (*green*) and RyR1 clusters (*red*) as yellow foci. The inset shows a fourfold enlarged area. Bar, 10 μm .

punctuate α_1 subunit fluorescence was co-localized with a similar RyR1 label (Fig. 1). The counts were obtained from several samples of at least three different experiments.

Patch-clamp and intracellular Ca^{2+} recording

Whole-cell patch-clamp recordings were performed with an Axopatch 200A amplifier controlled by pClamp 8.0 software (Axon Instruments Inc., Union City, CA, USA). The bath solution contained (mM): 10 CaCl_2 , 145 tetraethylammonium chloride, and 10 HEPES (pH 7.4 with TEA-OH). Patch pipettes, pulled from borosilicate glass (Harvard Apparatus, Kent, UK) had resistances of 1.8 to 2.5 $\text{M}\Omega$ when filled with 145 Cs-aspartate, 2 MgCl_2 , 10 HEPES, 0.1 Cs-EGTA, 2 Mg-ATP (pH 7.4 with Cs-OH). For simultaneous recording of whole-cell currents and Ca^{2+} transients the pipette solution additionally contained 0.2 mM fluo-4- K_5 (Molecular Probes). The Ca^{2+} fluorescence signal was recorded by a photometer system (PTI, S. Brunswick, NJ, USA) adjusted to the Zeiss Axiovert epifluorescence microscope. Ca^{2+} transients were normalized by the resting fluorescence ($\Delta F/F$). To attempt block of SR Ca^{2+} release, ryanodine and ruthenium red (both Sigma-Aldrich, Vienna, Austria) were dissolved in absolute ethanol or water, respectively, and added to the pipette solution at final concentrations of 10–40 μM for ryanodine and 10–160 μM for ruthenium red.

Leak currents were digitally subtracted by a P/4 prepulse protocol. Recordings were low-pass Bessel filtered at 1 kHz and sampled at 5 kHz. Currents were determined with 200 ms depolarizing steps from a holding potential of -80 mV to test potentials between -40 and $+80$ mV in 10 mV increments. Test pulses were preceded by a 1-s prepulse to -30 mV to

inactivate endogenous T-type Ca^{2+} currents (Adams et al., 1990). Current recordings of cells transfected with the T-type Ca^{2+} channel α_{1G} subunit were measured with 200 ms depolarizing steps from a holding potential of -90 mV to test potentials between -80 mV and $+80$ mV in 10 mV increments. Ca^{2+} current densities were normalized by linear cell capacitance and expressed in pA/pF.

Action potential-induced Ca^{2+} transients were recorded in cultures loaded for 45–60 min at room temperature with 5 μM fluo-4-AM plus 0.1% Pluronic F-127 (Molecular Probes) in HEPES and bicarbonate-buffered DME, as previously described (Flucher et al., 1993; Powell et al., 1996). Action potentials were elicited by passing 1 ms pulses of 30 V across the 19-mm incubation chamber. 0.5 mM Cd^{2+} and 0.1 mM La^{3+} were added to block Ca^{2+} influx and therefore allow discrimination between CICR and skeletal-type EC coupling. Application of 6 mM caffeine to the bath solution resulted in rapid Ca^{2+} release and thus proved the capacity of SR Ca^{2+} release.

Statistics

Data were expressed as mean \pm SE where n is the number of cells examined. Data analysis, unpaired Student's t -test, and one-way-ANOVA analysis followed by the Tukey post test were performed with Clampfit 8.0 (Axon instruments, Union City, CA, USA) and GraphPad Prism software (GraphPad Inc., San Diego, CA, USA). $P < 0.05$ was considered statistically significant.

RESULTS

It has previously been demonstrated that heterologous expression of different muscle α_1 subunit isoforms in dysgenic myotubes restores EC-coupling by two distinct mechanisms. Whereas the skeletal muscle α_{1S} triggers SR Ca^{2+} release independently of Ca^{2+} influx through the L-type Ca^{2+} channel, the cardiac α_{1C} depends on Ca^{2+} influx for activation of EC-coupling, presumably by CICR (Garcia et al., 1994). In contrast to the two muscle isoforms α_{1S} and α_{1C} , the neuronal non-L-type α_{1A} subunit was not capable of restoring EC-coupling in dysgenic myotubes, although α_{1A} generated sizable Ca^{2+} currents (Adams et al., 1994; Flucher et al., 2000). Here we expressed α_{1S} , α_{1C} , α_{1A} , and for the first time the L-type Ca^{2+} channel α_1 subunit isoform α_{1D} in dysgenic myotubes to compare their current properties and targeting characteristics with their ability to restore EC-coupling.

GFP- α_{1D} is targeted into triads of dysgenic myotubes

Immunofluorescence analysis (Fig. 1) shows that a fusion protein of GFP attached to the N-terminus of α_{1D} (GFP- α_{1D}) is efficiently expressed in myotubes of the dysgenic cell line GLT and is distributed in a clustered pattern. Double labeling of GFP- α_{1D} and RyR1 demonstrated that GFP- α_{1D} clusters were co-localized with clusters of RyR1, thus identifying the clusters as t-tubule/SR or plasma membrane/SR junctions, all of which will from here on be called triads. GFP- α_{1D} /RyR1 coclustering was found in 62% of 454 analyzed GFP- α_{1D} -expressing myotubes, which was similar to the degree of

clustering obtained with the native α_{1S} or with α_{1C} (see also Fig. 4 C). Myotubes in which GFP- α_{1D} was expressed in a nonclustered pattern typically showed ER/SR labeling (not shown), presumably because these myotubes were still very immature or due to unbalanced expression of the heterologous channel and endogenous muscle proteins (Flucher et al., 1994). Localizing GFP- α_{1D} (Fig. 1, green) in clusters coincident with the RyR (Fig. 1, red), makes α_{1D} the third member of the L-type Ca^{2+} channel family that, when expressed in skeletal muscle cells, is targeted into triads.

GFP- α_{1D} restores Ca^{2+} currents in dysgenic myotubes

Whole-cell patch-clamp measurements of dysgenic myotubes expressing GFP- α_{1D} revealed Ca^{2+} currents with properties distinct from those of GFP-tagged skeletal and cardiac α_1 subunits (Fig. 2). Myotubes were selected for electrophysiological analysis based on the GFP fluorescence. Ca^{2+} currents in response to depolarizing steps from a holding potential of -80 mV to voltages between -40 and $+80$ mV in 10 mM extracellular Ca^{2+} were recorded and used to calculate the current-to-voltage (I/V) relationship of GFP- α_{1D} . Representative current traces for the three α_1 subunit isoforms are shown in Fig. 2 C. Comparing the average I/V curves of GFP- α_{1D} currents to those of GFP- α_{1S} and GFP- α_{1C} expressed in dysgenic myotubes (Fig. 2 A) shows that the

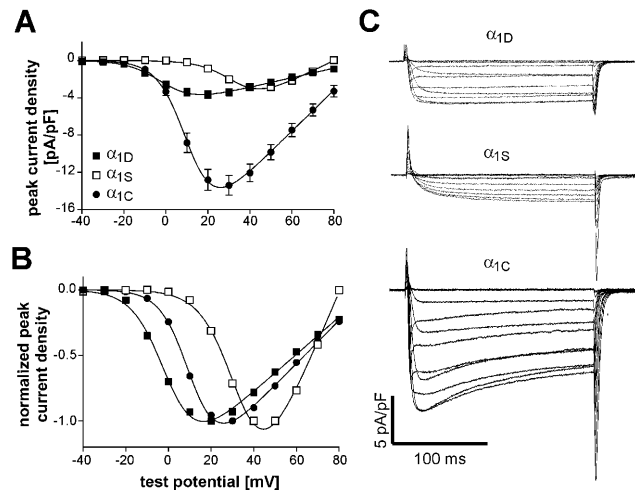


FIGURE 2 Current properties of GFP- α_{1D} expressed in dysgenic myotubes compared to those of GFP- α_{1S} and GFP- α_{1C} . (A) Voltage dependence of peak Ca^{2+} current densities (pA/pF; mean \pm SE) of GFP- α_{1D} (■; $n = 42$), GFP- α_{1S} (□; $n = 33$), and GFP- α_{1C} (●; $n = 28$). Maximal current density of GFP- α_{1D} is similar to that of GFP- α_{1S} and about four times lower than that of GFP- α_{1C} . (B) Normalized I/V curves show that GFP- α_{1D} activates at 13 mV more negative potentials than GFP- α_{1C} and at 37 mV more negative potentials than GFP- α_{1S} (for values of half maximal activation, see Table 1). (C) Representative whole-cell current recordings of GFP- α_{1D} , GFP- α_{1S} , and GFP- α_{1C} expressed in dysgenic myotubes. Cells were held at -80 mV and after a prepulse to inactivate low-voltage activated currents test pulses to increasing voltages from -40 to $+80$ mV were applied; currents were recorded in 10 mM Ca^{2+} . GFP- α_{1D} activates faster than GFP- α_{1S} .

TABLE 1 Properties of Ca^{2+} currents and Ca^{2+} transients recorded in reconstituted dysgenic myotubes with combined patch-clamp and fluo-4 Ca^{2+} measurements

α_1 -subunit	Current density (pA/pF)	G_{max} (nS/nF)	$V_{1/2}$ (mV)	k (mV)	$(\Delta F/F)_{\text{max}}$
α_{1D}	3.7 ± 0.4 (42)	51.3 ± 5.3	-0.6 ± 1.2	6.7 ± 0.3	0.27 ± 0.03 *** (9)
α_{1S}	3.1 ± 0.3 (33)	112.9 ± 6.8	36.0 ± 1.4	7.5 ± 0.3	0.96 ± 0.09 (34)
α_{1C}	14.1 ± 1.1 ** (28)	236.2 ± 20.2	12.2 ± 1.6	6.2 ± 0.4	0.30 ± 0.03 *** (10)
CSk53	22.3 ± 2.2 *** (35)	177.7 ± 18.0	5.9 ± 1.7	5.8 ± 0.5	0.41 ± 0.03 *** (18)
α_{1A}	24.1 ± 4.5 *** (18)	264.7 ± 55.9	6.0 ± 1.2	1.0 ± 0.2	0.50 ± 0.12 ** (12)

Entries correspond to mean \pm SE; numbers of cells are given in parentheses.

Significance (*** $P < 0.001$; ** $P < 0.01$) is given in relation to α_{1S} .

$(\Delta F/F)_{\text{max}}$ values other than that of α_{1S} are not significantly different from one another.

average maximal current density of GFP- α_{1D} is 3.7 ± 0.4 pA/pF, which is close to the value obtained with GFP- α_{1S} but significantly lower ($P < 0.01$) than the average current density of GFP- α_{1C} (Table 1). Furthermore, GFP- α_{1D} activates at more negative potentials than the two other α_1 subunits. The point of half-maximal activation for GFP- α_{1D} is ~ 13 mV more negative than that of GFP- α_{1C} and 37 mV more negative than that of GFP- α_{1S} (Table 1). The distinct activation characteristics can be best appreciated when the I/V curves are normalized for maximal amplitudes (Fig. 2 B). This analysis demonstrates that GFP- α_{1D} is functionally expressed in dysgenic myotubes and that its activation characteristics resemble those reported for α_{1D} in native cells and for GFP- α_{1D} in a nonmuscle expression system (Zidanic and Fuchs, 1995; Koschak et al., 2001).

GFP- α_{1D} restores cardiac-type EC-coupling in dysgenic myotubes

Next it was of interest to examine whether the small Ca^{2+} currents generated by GFP- α_{1D} would be sufficient to stimulate EC-coupling in dysgenic myotubes. This was first analyzed by recording intracellular Ca^{2+} signals in response to 1-ms current pulses passed through the recording chamber, in myotubes loaded with the fluorescent Ca^{2+} indicator fluo-4-AM. In normal myotubes and in dysgenic myotubes transfected with GFP- α_{1S} or GFP- α_{1C} , this field stimulation protocol has previously been shown to elicit Ca^{2+} transients with an all-or-none response to increasing voltages. This characteristic identifies the transients as action potential-induced Ca^{2+} transients (Flucher et al., 1993), which represent the most physiological parameter for assessing the restoration of EC-coupling. However, even in cultures transfected with the native GFP- α_{1S} , action potential-induced Ca^{2+} transients are observed only in a subset of expressing myotubes, presumably because excitability is achieved only in well differentiated cultured myotubes.

Cultures transfected with GFP- α_{1D} responded to field stimulation with brief Ca^{2+} transients (Fig. 3). The transients were characterized by a rapid upstroke that terminated abruptly, indicative of a strong voltage-dependence of both, the activation and the deactivation of the EC-coupling mechanism. The average amplitudes of the transients reached a

$(\Delta F/F)_{\text{max}}$ of 0.46 ± 0.04 , which was not significantly different from the amplitudes recorded with GFP- α_{1C} or GFP- α_{1S} (Table 2). The speed of the upstroke and the decay of the transients were similar between GFP- α_{1D} and GFP- α_{1C} ; however, the average values obtained with these channel isoforms were significantly slower than those of GFP- α_{1S} . Unless the expression of nonskeletal channels adversely affects the overall differentiation of the myotubes,

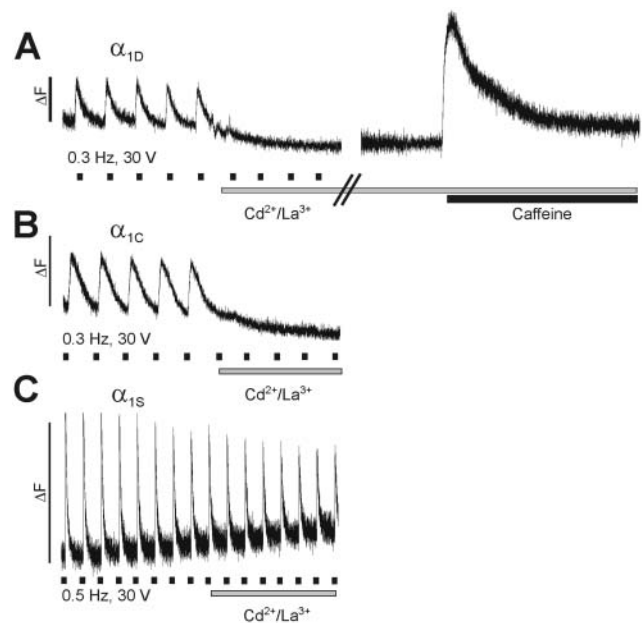


FIGURE 3 Restoration of action potential-induced Ca^{2+} transients by GFP- α_{1D} in dysgenic myotubes. Field stimulation at low frequency (30 V, 1 ms, 0.3 Hz/0.5 Hz) evoked rapid Ca^{2+} transients in myotubes expressing GFP- α_{1D} , GFP- α_{1C} , or GFP- α_{1S} . Bath application of 0.5 mM Cd^{2+} /0.1 mM La^{3+} immediately stopped the activation of transients in myotubes expressing GFP- α_{1D} (A) and GFP- α_{1C} (B), indicating that the transients were dependent on Ca^{2+} influx through the L-type channels. Addition of 6 mM caffeine (A, right trace) triggered a strong Ca^{2+} transient, proving that SR Ca^{2+} release was still functional during the Cd^{2+} / La^{3+} block. (C) Persistent Ca^{2+} transients after addition of Cd^{2+} / La^{3+} in myotubes expressing GFP- α_{1S} characterizes skeletal-type EC-coupling, which is independent of Ca^{2+} influx. In contrast, GFP- α_{1D} restored action potential-induced Ca^{2+} transients with cardiac characteristics. Marks underneath the traces indicate the approximate times of stimulation; bars indicate periods of Cd^{2+} / La^{3+} and caffeine application.

TABLE 2 Properties of action potential-induced Ca^{2+} transients recorded in reconstituted dysgenic myotubes with fluo-4 Ca^{2+} measurements

α_1 -subunit	Time to peak (s)	$(\Delta F/F)_{\text{max}}$	Decay time constant τ (s)	<i>N</i>
α_{1S}	0.068 ± 0.010	0.65 ± 0.09	0.255 ± 0.019	26
α_{1D}	0.370 ± 0.057 ***	0.46 ± 0.04	1.408 ± 0.170 ***	9
α_{1C}	0.257 ± 0.030 ***	0.55 ± 0.10	1.113 ± 0.103 ***	18

Entries correspond to mean \pm SE. Significance (***) $P < 0.001$ is given in relation to α_{1S} ; values of α_{1D} and α_{1C} are not significantly different from each other ($P > 0.05$).

for which there is no independent evidence based on the morphology of the myotubes and on the expression of proteins seen with immunocytochemistry, this difference in the time course of the transients probably reflects the different modes of EC-coupling (see below). But most important, despite the differences observed in the whole-cell current properties (Fig. 2), time-to-peak, amplitudes, and time constant of the decline of the Ca^{2+} transients were not significantly different ($P > 0.05$) between GFP- α_{1D} and GFP- α_{1C} (Table 2).

When Ca^{2+} currents were blocked by the addition of 0.5 mM Cd^{2+} /0.1 mM La^{3+} to the bath solution while continuously stimulating, the action potential-induced Ca^{2+} transients in GFP- α_{1D} -transfected myotubes ceased immediately (Fig. 3 A). This dependence of the Ca^{2+} transients on Ca^{2+} influx was similarly observed with GFP- α_{1C} (Fig. 3 B) and is the hallmark of cardiac-type EC-coupling. In contrast, because skeletal EC-coupling is independent of Ca^{2+} influx, blocking Ca^{2+} currents with Cd^{2+} / La^{3+} in myotubes transfected with GFP- α_{1S} did not stop action potential-induced Ca^{2+} transients (Fig. 3 C). To make sure that the inhibition of Ca^{2+} transients in myotubes expressing GFP- α_{1D} was indeed due to blocking the activation mechanism, SR Ca^{2+} release was tested by the application of 6 mM caffeine immediately after a blocking experiment. The strong Ca^{2+} release induced by caffeine (Fig. 3 A, right trace) showed that the failing response to field stimulation in Cd^{2+} / La^{3+} was not due to depletion of the SR or other effects on the release apparatus. Thus, GFP- α_{1D} restored cardiac-type EC-coupling in dysgenic myotubes.

Restoration of cardiac-type EC-coupling depends on triad targeting but not on the magnitude of the current density

In the field stimulation experiments GFP- α_{1D} was as efficient as GFP- α_{1C} in restoring action potential-induced Ca^{2+} transients in dysgenic myotubes. In Fig. 4 A we compare the frequencies at which action potential-induced Ca^{2+} transients were observed in cultures transfected with GFP- α_{1D} , GFP- α_{1C} , GFP- α_{1A} , and GFP- α_{1S} . The number of responding cells in cultures transfected with GFP- α_{1D} was not significantly different from those of GFP- α_{1C} and GFP- α_{1S} .

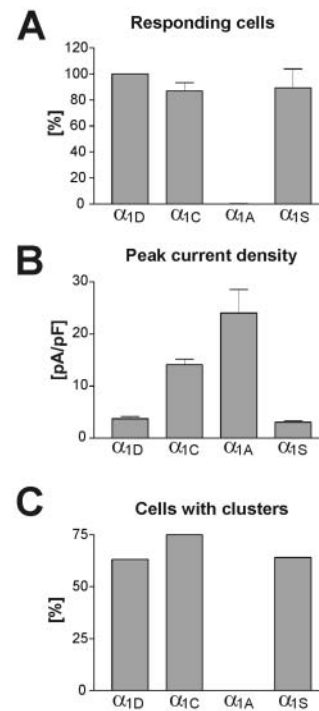


FIGURE 4 The ability of Ca^{2+} channel isoforms to restore EC-coupling compared to their current densities and targeting properties. (A) Myotubes responding to field stimulation with Ca^{2+} transients (see Fig. 3) were counted in cultures transfected with GFP- α_{1D} , GFP- α_{1C} , GFP- α_{1A} , and GFP- α_{1S} . Counts from seven experiments are expressed in percent (mean \pm SE) with the values of GFP- α_{1D} normalized to 100%. All three L-type channels (GFP- α_{1D} , GFP- α_{1C} , GFP- α_{1S}) restored EC-coupling with similar efficiency, whereas with GFP- α_{1A} only a single responding cell was observed. (B) Average peak current densities shown for the same channel isoforms as above (see also Table 1). Although the nonskeletal α_1 isoforms activate action potential-induced Ca^{2+} transients by CICR, no correlation of current density and restoration of EC-coupling exists (cf. A and B). (C) Fraction of myotubes in which the channel isoforms were targeted into the triads (see Fig. 1). The triad targeting properties of the Ca^{2+} channel isoforms exactly correspond to their ability to restore EC-coupling (cf. A and C).

As previously shown (Flucher et al., 2000), GFP- α_{1A} very rarely produced action potential-induced Ca^{2+} transients, probably due to the fact that this channel is not targeted into the triads. Out of six culture dishes transfected with GFP- α_{1A} , only a single myotube in one dish responded with an action potential-induced Ca^{2+} transient; therefore, the bar is not visible at this scale (Fig. 4 A). Comparing the capability of each of these channel isoforms to restore EC-coupling with the average densities of their Ca^{2+} currents shows no correlation of the two parameters (cf. Fig. 4, A and B). For GFP- α_{1S} , which directly activates SR Ca^{2+} release, such a correlation would not have been expected. However, for the constructs which elicit cardiac-type EC-coupling—presumably by CICR—a correlation of current density and their ability to activate action potential-induced Ca^{2+} transients was to be expected. Most interestingly, GFP- α_{1D} , with a current density of less than a third of that of GFP- α_{1C} , activated EC-coupling just as efficiently as the cardiac

channel. In contrast to current density, restoration of EC-coupling correlated very well with the triad targeting properties of the individual channel isoforms (cf. Fig. 4, A and C). Those constructs which are targeted into the triads (GFP- α_{1S} , GFP- α_{1C} , GFP- α_{1D}) all activated EC-coupling with similar efficiency. However GFP- α_{1A} , which generated the largest current density of all examined channel isoforms (see also Table 1) but is not targeted into triads, hardly ever activated action potential-induced Ca^{2+} transients in dysgenic myotubes. Thus, for the activation of cardiac-type EC-coupling, the spatial arrangement of the Ca^{2+} channels opposite the RyR appears to be more important than the pure size of the Ca^{2+} currents.

Ca^{2+} transients activated by GFP- α_{1C} and GFP- α_{1D} are qualitatively and quantitatively different from those activated by GFP- α_{1S}

To further characterize the dependence of cardiac-type EC-coupling on Ca^{2+} currents we performed combined patch-clamp and fluo-4 Ca^{2+} recording experiments in dysgenic myotubes expressing different α_1 subunit isoforms. This approach enables us to simultaneously monitor the whole-cell Ca^{2+} influx and intracellular Ca^{2+} transients in the same myotubes, and it allows us to analyze the voltage-dependence of Ca^{2+} transients. But these experiments differ from the analysis of action potential-induced Ca^{2+} transients in several important aspects: 1), Sampling—whereas with field stimulation we see and record only those myotubes that have achieved excitability and a good degree of EC-coupling (probably the peak of the population of expressing cells), with the patch-clamp approach we get a random sample of differently well developed and expressing myotubes; 2), Stimulation—instead of a 1-ms extracellular current pulse, which stimulates an action potential lasting only a few milliseconds, in the patch-clamp experiments we depolarize the cells for 200 ms giving rise to unnaturally long periods of Ca^{2+} influx; and 3), Intracellular milieu—while the myotube is being loaded with the Ca^{2+} indicator through the patch pipette, the cells are dialyzed and Ca^{2+} buffers and the entire intracellular milieu are altered. Thus, in this set of experiments we trade in better control and quantitative analysis for less physiological conditions. This is reflected in the shape of the Ca^{2+} transients in response to the 200-ms depolarization (Fig. 5 C), which does not resemble that of action potential-induced Ca^{2+} transients (Fig. 3).

Nevertheless, important functional characteristics of the transients, like the skeletal- and cardiac-type activation of EC-coupling, can be distinguished in the voltage-dependence curves of Ca^{2+} transients (Garcia et al., 1994). The amplitudes of Ca^{2+} transients stimulated by GFP- α_{1C} mirror those of the Ca^{2+} currents over a wide voltage range (Figs. 5, A and B). In contrast, with GFP- α_{1S} Ca^{2+} transients activate at more negative potentials as the Ca^{2+} currents and stay fully activated at voltages near the reversal potential where

currents decline. As expected from the dependence of action potential-induced Ca^{2+} transients on Ca^{2+} influx shown in Fig. 3, the voltage-dependence curves of Ca^{2+} transients in myotubes expressing GFP- α_{1D} showed the cardiac characteristics (Fig. 5 A). With this construct the Ca^{2+} transients activated in parallel with the currents at more negative potentials than those of GFP- α_{1C} and declined at voltages above +20 mV. Interestingly, the maximal amplitudes of the transients for GFP- α_{1D} and GFP- α_{1C} were not significantly different ($P > 0.05$) despite the more than threefold difference in current densities (Fig. 5; Table 1). This suggests that currents of both channels reach the activation threshold of CICR and trigger equal amounts of Ca^{2+} release. However, the maximal amplitudes of the Ca^{2+} transients activated by GFP- α_{1D} or GFP- α_{1C} were much lower than that activated by GFP- α_{1S} . This indicates that the native channel either activates a larger Ca^{2+} pool or activates SR Ca^{2+} release more efficiently than the two nonskeletal channel isoforms.

Unexpectedly, also GFP- α_{1A} , which in the field stimulation experiments restored action potential-induced Ca^{2+} transients very rarely (Fig. 4 A), frequently produced cardiac-type Ca^{2+} transients in the combined patch-clamp/fluo-4 Ca^{2+} recording experiments. Apparently the mechanism that limited activation of cardiac-type EC-coupling in response to action potential-induced Ca^{2+} transients to the correctly targeted channel isoforms broke down under the conditions of the patch-clamp experiments. But even in this case, the average maximal amplitudes of Ca^{2+} transients were similar to those of GFP- α_{1C} and GFP- α_{1D} (Fig. 5). Whereas the transient-to-voltage relationship for GFP- α_{1A} is somewhat higher than that of GFP- α_{1C} and GFP- α_{1D} (Table 1), this difference is not statistically significant ($P > 0.05$) and mainly reflects a single recording with an exceptionally high current and transient. If this recording is excluded from the analysis, the transients of GFP- α_{1A} are also in the exact same range as GFP- α_{1D} and GFP- α_{1C} (dotted curve in Fig. 5 A). At this point we have no explanation for the occurrence of such exceptionally strong responders. However, one needs to remember that also in the field stimulation experiments occasional responders were observed with GFP- α_{1A} (see above; Adams et al., 1994; Flucher et al., 2000).

Analysis of the combined patch-clamp/fluo-4 Ca^{2+} recording experiments revealed striking differences between the skeletal and nonskeletal α_1 subunits expressed in dysgenic myotubes. Plotting the amplitudes of the Ca^{2+} transients versus the peak current densities for all individual experiments (Fig. 5 D) shows that dysgenic myotubes reconstituted with GFP- α_{1S} produce Ca^{2+} transients of greatly variable size ($\Delta F/F$ values up to 2.60) with no correlation to current densities. Ca^{2+} transients are observed even in myotubes with no detectable currents, and some of the myotubes with the highest current densities showed very small transients. In contrast, GFP- α_{1C} and GFP- α_{1D} display a completely different picture. Data points of both channels spread out over a wide range of current densities but within

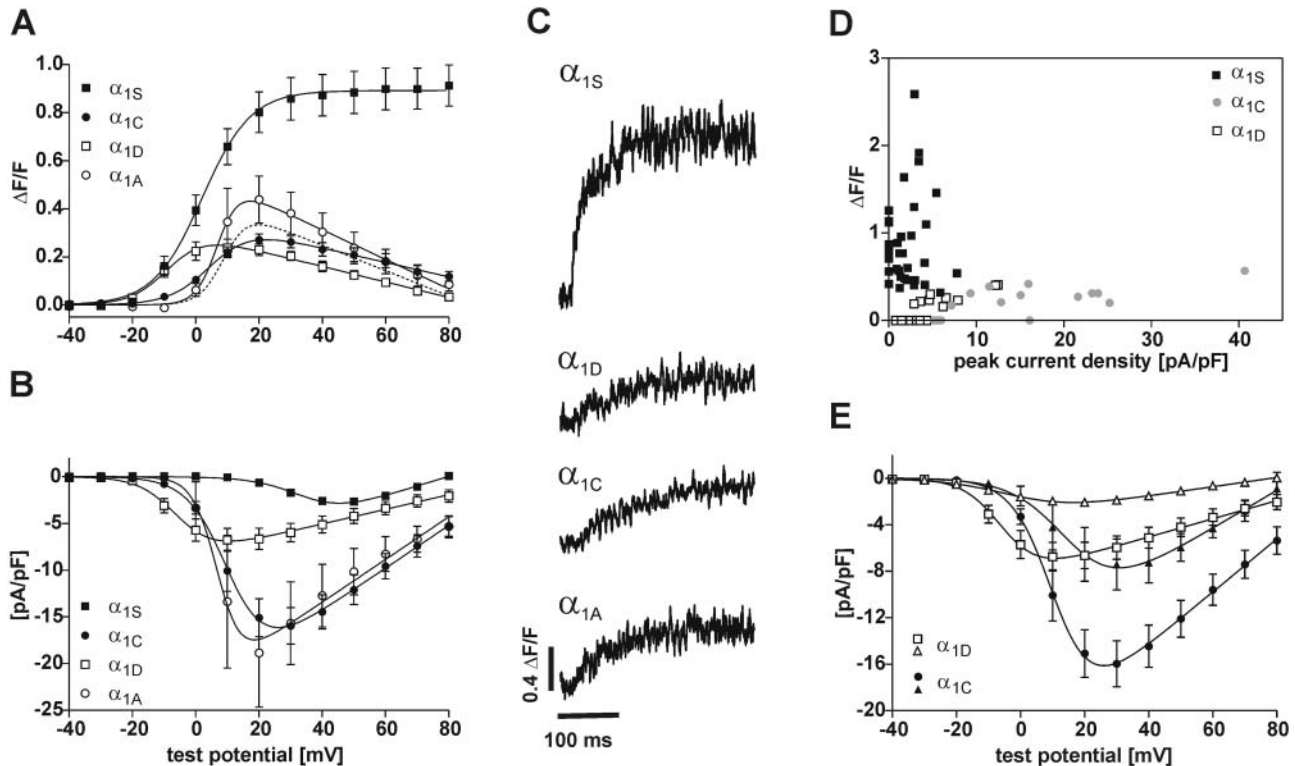


FIGURE 5 Simultaneous recording of whole-cell Ca^{2+} currents and Ca^{2+} transients in dysgenic myotubes transfected with skeletal and nonskeletal α_1 subunit isoforms. (A, B) Voltage-dependence of Ca^{2+} transients (A) and of Ca^{2+} currents (B). Ca^{2+} transients of GFP- α_{1S} (■; $n = 34$) have a sigmoidal voltage relationship that does not follow the I/V curve. Transient-to-voltage curves for GFP- α_{1C} (●; $n = 10$), GFP- α_{1D} (□; $n = 9$), and GFP- α_{1A} (○; $n = 11$) are bell-shaped and follow their I/V curves with respect to activation properties but not with respect to amplitudes. Whereas current densities for GFP- α_{1D} are significantly smaller than those of GFP- α_{1C} ($P = 0.0011$) or GFP- α_{1A} ($P = 0.014$), their maximal amplitudes of Ca^{2+} transients are not significantly different from each other ($P > 0.05$). The dotted line shows the shift in the GFP- α_{1A} I/V curve after removing one exceptionally high recording from the analysis. But transients of all nonskeletal isoforms are significantly smaller ($P < 0.001$) than that of GFP- α_{1S} . (C) Representative examples of Ca^{2+} transients recorded with fluo-4 in parallel to whole-cell currents show the difference between skeletal and nonskeletal α_1 isoforms. (D) A scatter plot of the maximal peak current densities versus peak $\Delta F/F$ values for GFP- α_{1S} (■), GFP- α_{1C} (●), and GFP- α_{1D} (□) shows that skeletal and nonskeletal Ca^{2+} signals clearly separate into two distinct groups. Suprathreshold Ca^{2+} transients of GFP- α_{1C} and GFP- α_{1D} are confined to a narrow window of amplitudes over a wide range of current densities. (E) I/V curves of GFP- α_{1C} (●) and GFP- α_{1D} (□) (both the same as in B) compared to the average I/V curves of those currents for each group, which did not evoke Ca^{2+} transients (▲, GFP- α_{1C} , $n = 5$; △, GFP- α_{1D} , $n = 16$). For both channels, currents without transients were relatively smaller than those that evoked transients, but the absolute values differed significantly.

a relatively narrow window of Ca^{2+} transient amplitudes ($\Delta F/F$ values between 0.15 and 0.42). The maximal transient amplitudes of both nonskeletal channel isoforms do not reach those of the skeletal GFP- α_{1S} .

Furthermore, a fraction of GFP- α_{1C} - and GFP- α_{1D} -expressing myotubes showed Ca^{2+} currents but no detectable Ca^{2+} transient (33% and 64% of myotubes expressing GFP- α_{1C} and GFP- α_{1D} , respectively). This was never the case with GFP- α_{1S} . In Fig. 5 E a second set of I/V curves is shown for GFP- α_{1C} and GFP- α_{1D} . In addition to the I/V curve of those myotubes responding with both currents and transients (same as in Fig. 5 B), I/V curves were calculated from those recordings, in which Ca^{2+} currents were not accompanied with Ca^{2+} transients. For both channel isoforms the currents not associated with Ca^{2+} transients were significantly smaller (α_{1D} : $P = 0.0001$; α_{1C} : $P = 0.0180$) than those associated with transients. Thus, in both cases the larger currents activated transients whereas the smaller

currents did not. This could be interpreted as the existence of a threshold for triggering the Ca^{2+} signal. However, the whole-cell current densities necessary to activate Ca^{2+} transients differed greatly between the two channel isoforms. The amplitudes of Ca^{2+} currents of GFP- α_{1D} that were associated with Ca^{2+} transients were almost identical to those of GFP- α_{1C} that were not associated with transients (Fig. 5 E). Thus, whereas current amplitudes matter for the activation of Ca^{2+} release in skeletal myotubes, the absolute values of whole-cell current densities do not reliably describe the activation threshold in the triad.

The two distinct groups of Ca^{2+} transient amplitudes do not depend on the skeletal versus cardiac EC-coupling mechanisms

The data presented above show that GFP- α_{1C} and GFP- α_{1D} expressed in dysgenic myotubes give rise to Ca^{2+} transients

with an average maximal amplitude at about one third of that activated by GFP- α_{1S} (Table 1). Therefore it was reasonable to assume that the difference in skeletal versus cardiac EC-coupling mechanisms (direct or Ca^{2+} -dependent) is responsible for this striking difference. This hypothesis was tested with a channel chimera, GFP-CSk53, which consists of GFP- α_{1C} with a 46-amino-acid sequence in the II-III cytoplasmic loop replaced by the corresponding sequence of α_{1S} (Nakai et al., 1998). This sequence is sufficient to confer skeletal-type EC-coupling properties onto the cardiac channel. Action potential-induced Ca^{2+} transients persist after application of $\text{Cd}^{2+}/\text{La}^{3+}$ to block Ca^{2+} currents (Fig. 6 E). This observation is in agreement with earlier reports showing that GFP-CSk53 activated EC-coupling by the skeletal Ca^{2+} -independent mechanism (Nakai et al., 1998). Fig. 6, A–D shows the voltage-dependence of Ca^{2+} transients and currents of GFP-CSk53 compared to those of GFP- α_{1S} and GFP- α_{1C} . Peak current densities similar to those of GFP- α_{1C} (Fig. 6 B; Table 1) demonstrate the normal functional expression of the channel chimera. But surprisingly, on first sight the voltage relationship of the transients of GFP-CSk53 resembled that of the cardiac and not of the skeletal isoforms in both amplitude and shape (Fig. 6 A). However, the analysis of individual recordings from the

combined patch-clamp/fluo-4 Ca^{2+} experiments showed that the cardiac-like decline of the transients at voltages above +20 mV was preferentially seen in those recordings where the baseline shifted upward during the duration of the experiment. Dividing the recordings into those with baseline shifts below and those above 10% (Fig. 6 C) revealed that the records with little or no shift displayed the typical skeletal characteristics of the voltage-dependence of the Ca^{2+} transients, i.e., no decline at higher test potentials. The same analysis performed with the recordings of GFP- α_{1C} showed typical cardiac characteristics in both groups (Fig. 6 D). Therefore, the apparent decline of the amplitudes of Ca^{2+} transients at positive potentials was an experimental artifact that could be avoided by excluding the data of recordings with a baseline shift greater than 10%.

GFP-CSk53 activates Ca^{2+} transients by the skeletal mechanism

Nevertheless, its maximal Ca^{2+} transient amplitudes were similar to those of the nonskeletal α_1 subunits (Fig. 6, A and F). The average maximal amplitude of Ca^{2+} transients for GFP-CSk53 was 0.41 ± 0.03 , which is not significantly different from those of GFP- α_{1C} and GFP- α_{1D} but sig-

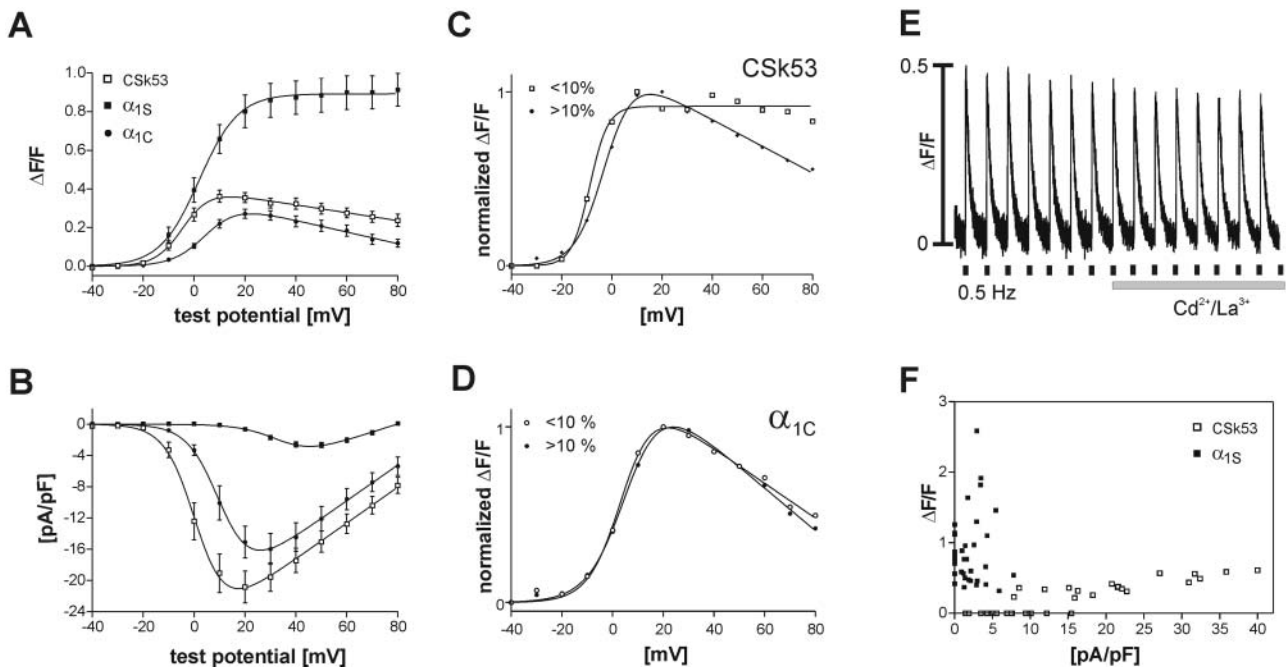


FIGURE 6 Comparison of the cardiac-skeletal chimera CSk53 with α_{1C} and α_{1S} . The voltage-dependences of Ca^{2+} transients (A) and of peak current densities (B) of CSk53 (\square , $n = 18$) resemble in size and shape those of GFP- α_{1C} (\bullet) but not those of GFP- α_{1S} (\blacksquare). The bell-shaped (cardiac-type) Ca^{2+} transient-to-voltage curve of CSk53 is in disagreement with skeletal-type EC-coupling properties as indicated by the insensitivity of action potential-induced Ca^{2+} transients to $\text{Cd}^{2+}/\text{La}^{3+}$ block (E). (C) Dividing the CSk53 records into two groups based on the occurrence and magnitude of a fluorescence baseline shift (above and below 10%) shows that the stable recordings (baseline shift < 10%; \square , $n = 7$; > 10%, \blacklozenge , $n = 11$) display a sigmoidal transient-to-voltage relationship. (D) In contrast, the transient-to-voltage curves of α_{1C} are bell-shaped regardless of the size of a baseline shift (baseline shift < 10%, \circ , $n = 5$; > 10%, \bullet , $n = 5$). Therefore, the bell-shaped appearance of the curve for CSk53 in A is due to this artifact, and the true character of the CSk53 transients is skeletal. (F) A scatter plot of maximal peak current densities versus $\Delta F/F$ values emphasizes the difference between Ca^{2+} transients of CSk53 and GFP- α_{1S} . Whereas current densities for CSk53 vary between 1.5 and 40 pA/pF, the amplitudes of the transients do not exceed $\Delta F/F$ values of 0.6.

nificantly lower than that of GFP- α_{1S} ($P < 0.001$; Table 1). Thus, the difference in amplitudes of Ca^{2+} transients observed in myotubes transfected with GFP- α_{1C} and GFP- α_{1D} on one hand, and with GFP- α_{1S} on the other, cannot be solely explained by the difference between the cardiac and skeletal activation mechanisms.

Cardiac-type and skeletal-type Ca^{2+} transients can be individually activated in the same myotube

Finally, we wanted to exclude the possibility that the relatively low Ca^{2+} transients in myotubes transfected with nonskeletal muscle α_1 subunit isoforms and the chimera CSk53 were simply due to a reduced Ca^{2+} release capacity of those myotubes. Therefore we examined whether the same myotube responded with different size Ca^{2+} transients when activated by the native GFP- α_{1S} or by a nonskeletal channel. The low-voltage-activated Ca^{2+} channel GFP- α_{1G} (Monteil et al., 2000) also gave rise to Ca^{2+} transients in dysgenic myotubes. These activated at potentials of -60 mV and peaked at about -40 mV, both at ~ 40 mV more negative potentials than transients in GFP- α_{1S} -expressing myotubes (Fig. 7 A). Similar to the Ca^{2+} transients of all other examined nonskeletal α_1 subunits, GFP- α_{1G} transients reached maximal amplitudes that were substantially smaller than those of GFP- α_{1S} . When coexpressed with GFP- α_{1S} , Ca^{2+} transients activated by GFP- α_{1G} could be well separated from transients activated by the high-voltage-activated GFP- α_{1S} (Fig. 7 C). The transient-to-voltage curve of cotransfected myotubes displayed a shoulder at -30 mV and continued to rise at -10 mV (Fig. 7 A). Subtracting the transient-to-voltage curve of GFP- α_{1G} alone from that of the cotransfection experiments eliminated the shoulder, resulting in a curve with typical skeletal characteristics (Fig. 7 B). Thus, we conclude that the shoulder represents the contribution of GFP- α_{1G} . The height of this shoulder is near $\Delta F/F$ values of 0.3, which corresponds to transients observed with GFP- α_{1C} , GFP- α_{1D} , GFP- α_{1A} , and GFP-CSk53, and it is only about one third of the maximal Ca^{2+} signal activated by GFP- α_{1S} in the same cells at more positive voltages. Thus, in our experiments Ca^{2+} transients activated by channels other than the native GFP- α_{1S} peak at amplitudes significantly below that activated by GFP- α_{1S} , even in the same myotube.

DISCUSSION

In this study we investigated the properties of “cardiac-type” EC-coupling activated in skeletal muscle cells by reconstituting dysgenic myotubes with nonskeletal α_1 subunit isoforms. GFP- α_{1D} —an L-type Ca^{2+} channel isoform found in pancreatic β cells, hair cells of the cochlea, and in the sinus node of the heart (Hell et al., 1993; Iwashima et al., 1993; Kollmar et al., 1997; Takimoto et al., 1997)—was targeted into the triads and restored action potential-induced

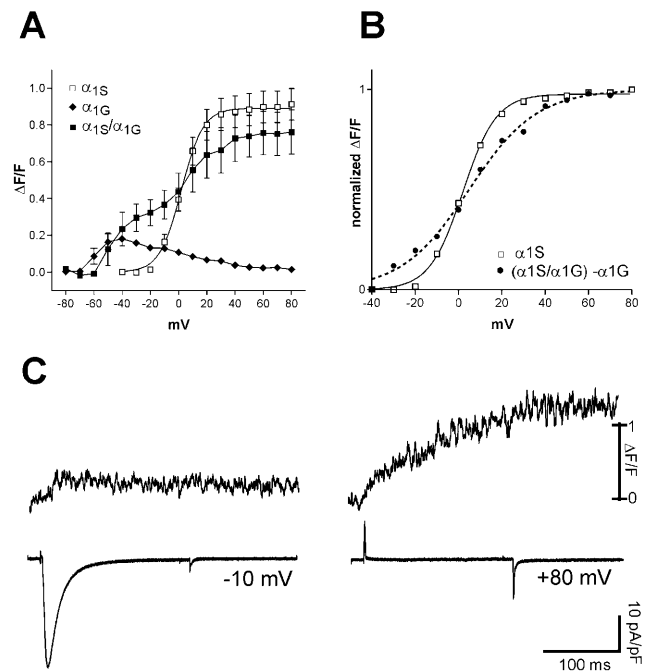


FIGURE 7 Cardiac-type and skeletal-type EC-coupling activated independently in the same myotube. (A) Voltage-dependence of Ca^{2+} transients in dysgenic myotubes transfected with GFP- α_{1G} alone (\blacklozenge ; $n = 9$) and in combination with GFP- α_{1S} (\blacksquare ; $n = 9$). The low-voltage activated Ca^{2+} channel GFP- α_{1G} generates cardiac-type Ca^{2+} transients activated at negative voltages with maximal amplitudes ($\Delta F/F$) not significantly different from those of GFP- α_{1C} and GFP- α_{1D} (cf. Fig. 5). The I/V curve of cotransfected myotubes displays a shoulder at negative potentials and continues to rise at positive potentials to levels similar to those achieved with GFP- α_{1S} alone (\square ; data from Fig. 5 A). Maintained transients at $+80$ V near the reversal potential characterize this component as skeletal. (B) Subtraction of the I/V curve of GFP- α_{1G} from that of the GFP- α_{1G} /GFP- α_{1S} -cotransfected myotubes results in a curve (\bullet) resembling that of GFP- α_{1S} (\square). (C) Examples of Ca^{2+} transients and currents from a cotransfected cell depolarized to -10 mV (left traces) and to $+80$ mV (right traces). Ca^{2+} -dependent (cardiac-type) and Ca^{2+} -independent (skeletal-type) transients can be activated independently from each other in the same cell.

Ca^{2+} transients as efficiently as GFP- α_{1C} , even though its whole-cell current density was much smaller. In combined patch-clamp/fluo-4 measurements, Ca^{2+} transients activated by GFP- α_{1C} and GFP- α_{1D} peaked at amplitudes significantly below those of the skeletal GFP- α_{1S} . However, this difference in the size of Ca^{2+} transients was not due to the different EC-coupling activation mechanisms, because CSk53, a cardiac channel with skeletal EC-coupling characteristics, also gave rise to transients of reduced magnitude.

GFP- α_{1D} , together with the native α_{1S} and the cardiac α_{1C} , is now the third member of the voltage-gated Ca^{2+} channel family that has been demonstrated to become normally targeted into the skeletal muscle triads. Apparently all the members of the L-type subclass so far examined possess the triad targeting signals, whereas the neuronal, non-L-type α_{1A} does not (Flucher et al., 2000). We have previously shown that an important triad targeting signal resides

in the C-terminus of α_{1S} and can be conferred onto GFP- α_{1A} by replacing a short C-terminal sequence with the corresponding sequence of α_{1S} (Flucher et al., 2000). Similarly the C-terminus of GFP- α_{1D} was able to confer triad targeting properties onto GFP- α_{1A} (Flucher and Grabner, unpublished results). Thus, triad targeting signals could be a conserved property of the L-type Ca^{2+} channel family. Alternatively, since α_{1S} , α_{1C} , and α_{1D} isoforms are all expressed in various muscle tissues whereas α_{1A} is not, the triad targeting property could be a muscle-specific feature.

Ca^{2+} currents generated by GFP- α_{1D} expressed in dysgenic myotubes showed the typical characteristics previously reported for α_{1D} in native cells (Zidanic and Fuchs, 1995) and of GFP- α_{1D} expressed in mammalian heterologous expression systems (Koschak et al., 2001). GFP- α_{1D} currents activated at 13 mV more negative potentials compared to GFP- α_{1C} . The current density of GFP- α_{1D} in dysgenic myotubes was less than one third of that of GFP- α_{1C} . Nevertheless, both channels restored action potential-induced Ca^{2+} transients in dysgenic myotubes equally well and as efficiently as the native GFP- α_{1S} . The fact that these Ca^{2+} transients were blocked by $\text{Cd}^{2+}/\text{La}^{3+}$ demonstrated that the mechanism by which GFP- α_{1D} activated action potential-induced Ca^{2+} transients was CICR, with the trigger Ca^{2+} provided by the L-type Ca^{2+} current. Therefore it was surprising that the considerable difference in the size of the currents of GFP- α_{1D} and GFP- α_{1C} was not reflected in the size of the transients or in the rate at which action potential-induced Ca^{2+} transients were observed. Thus, activation of CICR is not strongly dependent on the total influx of Ca^{2+} manifested in the whole-cell current densities. This conclusion is further supported by data on α_{1A} collected by us and others (Adams et al., 1994; Flucher et al., 2000; and present study). While α_{1A} expressed in dysgenic myotubes produces high current densities the size of GFP- α_{1C} or larger, it restores contractions or action potential-induced Ca^{2+} transients very rarely.

Whereas the ability of the examined α_1 subunits to trigger Ca^{2+} transients does not correlate with the magnitude of their Ca^{2+} currents, it correlates well with their triad targeting properties. All channel isoforms that are efficiently targeted into the triads (GFP- α_{1S} , GFP- α_{1C} , GFP- α_{1D}) also restore action potential-induced Ca^{2+} transients. On the other hand, GFP- α_{1A} fails to do either. This suggests that activation of EC-coupling by CICR is dependent on local Ca^{2+} concentrations achieved in the restricted space of the triad in the moment of depolarization by an action potential. In the triad, even the small GFP- α_{1D} currents—which are of similar size as those of α_{1S} —attain the concentration necessary for activating SR Ca^{2+} release. However, the Ca^{2+} activation threshold of Ca^{2+} release is not reached during fivefold larger Ca^{2+} currents generated by the nontargeted GFP- α_{1A} channel isoform. A local activation mechanism for CICR is also consistent with the observation that the termination of the Ca^{2+} release during action potential-induced Ca^{2+}

transients is under the tight control of the membrane potential. At least in the dysgenic system, CICR is not a regenerative process that is self-sustained by Ca^{2+} released through the RyRs alone. In that case transients would be expected to continue to rise after repolarization and the deactivation of voltage-gated Ca^{2+} channels. On the contrary, the abrupt termination of the transients upon repolarization argues that the sustenance of the CICR requires the continued influx of Ca^{2+} through a voltage-gated channel. This tight control of Ca^{2+} activation of the Ca^{2+} release channels by voltage-gated Ca^{2+} currents in dysgenic myotubes reconstituted with GFP- α_{1C} or GFP- α_{1D} is reminiscent of EC coupling in cardiac myocytes (Cannell et al., 1987; Stern et al., 1999; Bers, 2000) and can only be envisioned in the restricted space of the triad junction, where α_{1C} or α_{1D} come within nanometers of the Ca^{2+} release channel (Rios and Stern, 1997).

A role of local Ca^{2+} gradients in the activation of CICR in skeletal myotubes is further corroborated by the observation that the lower limits of current densities required for triggering Ca^{2+} transients differ between GFP- α_{1C} and GFP- α_{1D} . In both cases failure of activation of Ca^{2+} transients was preferentially observed in myotubes with low current densities, whereas the myotubes with higher current densities usually produced Ca^{2+} transients. However, the current density required for the activation of Ca^{2+} transients was not constant. It varied between individual myotubes, and it was clearly different between GFP- α_{1C} and GFP- α_{1D} . The existence of a threshold of current density below which no Ca^{2+} release would be stimulated is expected for CICR. But this threshold should be the same in myotubes expressing GFP- α_{1C} and GFP- α_{1D} . Thus, we have to conclude that the whole-cell current densities only incompletely reflected the actual Ca^{2+} concentration at the activation site. Either the geometry of the channels in the triad is such that the spatiotemporal Ca^{2+} gradients required for Ca^{2+} activation of the RyR are similar for GFP- α_{1C} and GFP- α_{1D} even though their channel properties differ or, alternatively, the fractions of channels inside and outside the triad might differ for the two α_1 isoforms, so that there is no linear relationship between whole-cell current densities and current densities in the triads.

GFP- α_{1A} , which is not targeted into triads and usually fails to trigger action potential-induced Ca^{2+} transients, generated Ca^{2+} transients in the combined patch-clamp and fluo-4 Ca^{2+} recording experiments. On first sight, this result appears to contradict the hypothesis that triggering cardiac-type EC-coupling by CICR depends on the co-localization of the t-tubular and SR Ca^{2+} channels in the triads. However, if activation of CICR in the triads depends on local Ca^{2+} gradients, these could easily break down during the 200-ms depolarization of the patch-clamp experiments. During a brief action potential locally high Ca^{2+} concentrations near the mouth of a channel may activate SR Ca^{2+} release in the case of channels concentrated in the triad junction, whereas similarly high Ca^{2+} concentrations generated by

α_{1A} channels diffusely located outside the triads may dissipate in the highly buffered cytoplasm before reaching the RyRs in the triad. However, during continued activation over the period of 200 ms, Ca^{2+} entering the myotube through α_{1A} may flood the cell to a degree that spatial gradients can no longer be maintained and CICR is triggered even by a channel positioned outside the triad. Interfering with the Ca^{2+} buffering milieu in the patched myotubes may further contribute to this inconsistent behavior under the different experimental conditions. The different shapes of Ca^{2+} transients produced by the field stimulation and in the combined patch-clamp recordings support this explanation (see also Garcia et al., 1994). The fact that in these experiments Ca^{2+} transients do not decline immediately after repolarization suggests that in contrast to action potential-induced Ca^{2+} transients, CICR stimulated by long depolarization contains a regenerative component, which sustains Ca^{2+} release even in the absence of influx. Also the slow decline of the Ca^{2+} transients indicates that the cytoplasmic Ca^{2+} buffering capacity has been exceeded under these experimental conditions. Applying shorter test pulses (10 ms) partially reversed this problem, and Ca^{2+} transients looked more like those of the action potential-induced Ca^{2+} transients (not shown). However, analyzing the voltage-dependence of current and transient activation and a reliable comparison of current densities of channels with different activation kinetics necessitated long depolarization. Therefore, even though analysis of Ca^{2+} signals under voltage-clamp control is common practice and has contributed significantly to our current understanding of EC-coupling (e.g., Baylor et al., 1983; Brum et al., 1987; Melzer et al., 1984; Beurg et al., 1997; Dietze et al., 1998; Jurkat-Rott et al., 1998; Grabner et al., 1999; Wilkens et al., 2001), it has to be kept in mind that spatiotemporal Ca^{2+} gradients, which appear to be critical for activation of CICR under physiological conditions, probably break down during prolonged patch-clamp recordings.

A trivial alternative explanation for the different size, shape, and behavior of Ca^{2+} transients obtained with patch-clamp stimulation would be that the transients recorded from nonskeletal Ca^{2+} channels in the patch-clamp mode are not CICR at all, but simply reflect the Ca^{2+} influx through these channels. This would explain the reduced amplitude compared to that of the skeletal transients as well as the fact that GFP- α_{1A} , which failed to restore action potential-induced Ca^{2+} transients, generates a Ca^{2+} signal under patch-clamp conditions. Attempts to test this possibility by pharmacologically isolating a possible Ca^{2+} influx signal from that of CICR did not resolve the issue either, because even concentrations between 10 μM and 40 μM ryanodine (Lipp et al., 2002) or 10 μM and 160 μM ruthenium red (Xu et al., 1999) in the patch pipette did not completely block Ca^{2+} release in control myotubes transfected with GFP- α_{1S} . However, important evidence from this and previous studies (Tanabe et al., 1990; Garcia et al., 1994; Garcia and Beam,

1994) argues against the possibility that these Ca^{2+} transients arise exclusively from Ca^{2+} influx: first, the poor correlation of current densities with the occurrence of associated Ca^{2+} transients in individual myotubes; i.e., myotubes with current densities as small as 3 pA/pF showed transients whereas other myotubes with much larger currents showed no measurable transients (Fig. 5 D) (see also Garcia et al., 1994); second, the poor correlation of current densities with the amplitudes of Ca^{2+} transient for GFP- α_{1C} and GFP- α_{1D} , i.e., whereas their current densities differed by almost threefold, GFP- α_{1C} and GFP- α_{1D} produced Ca^{2+} transients of similar magnitude (Fig. 5, A and B); and finally, Ca^{2+} transients triggered by the cardiac-skeletal chimera GFP-CSk53 were not significantly larger than those of GFP- α_{1C} , as would be expected from a construct that triggers skeletal-type Ca^{2+} release in addition to a fluo-4 signal reflecting pure Ca^{2+} influx. If we had merely recorded the influx of Ca^{2+} , the magnitude of the Ca^{2+} transients should be highly correlated to the underlying currents. On the contrary, the behavior of the observed Ca^{2+} transients is consistent with a CICR mechanism that depends not only on the size of the Ca^{2+} influx but also on its local density.

Comparing the voltage-dependence of the Ca^{2+} currents with that of the Ca^{2+} transients revealed important properties of CICR in skeletal myotubes. For the nonskeletal channels, the voltage-dependence of the Ca^{2+} transients faithfully followed that of the current density, resulting in the bell-shaped curve typical for cardiac-type EC-coupling (Tanabe et al., 1990). Moreover, differences in the voltage-dependence of the currents, like the left-shifted activation of GFP- α_{1D} , can similarly be observed for the transients. This strict correlation of current amplitudes and transient amplitudes at different voltages clearly indicates that CICR is not simply an all-or-none mechanism. Smaller currents give rise to smaller transients and larger currents give rise to larger transients. Thus, CICR in individual skeletal myotubes functions as a graded amplification system in which Ca^{2+} entering the myotube through the voltage-gated channels is proportionally amplified by Ca^{2+} released from the SR. Nevertheless, considerable differences in current densities between individual cells and the differences in the average current densities of GFP- α_{1C} and GFP- α_{1D} are not reflected in the maximal amplitudes of the transients. These are very similar in all myotubes expressing nonskeletal α_1 subunits, and they peak at a level way below the maximal capacity of SR Ca^{2+} release. Thus, it seems that irrespective of their different current properties, GFP- α_{1C} , GFP- α_{1D} , GFP- α_{1A} , and GFP- α_{1G} activate the same maximal amount of Ca^{2+} release in the combined patch-clamp/fluo-4 recordings.

This reduced maximum of Ca^{2+} release achieved by the nonskeletal channels is, however, not due to a limited release capacity of the EC-coupling apparatus. Ca^{2+} transients activated by GFP- α_{1S} were on average three times larger than those of nonskeletal channels. This observation is consistent with similar differences seen in an earlier report comparing

α_{1S} and α_{1C} expressed in myotubes of dysgenic primary cultures (Garcia et al., 1994). But perhaps myotubes reconstituted with the skeletal GFP- α_{1S} channel differentiate better than myotubes expressing the heterologous channel isoforms and therefore generate more robust Ca^{2+} transients? However, even on a single myotube level we observed that non-skeletal Ca^{2+} channels released only a fraction of the Ca^{2+} releasable by GFP- α_{1S} . Myotubes cotransfected with a low-voltage-activated channel GFP- α_{1G} and the high-voltage-activated GFP- α_{1S} showed the typical small cardiac-type Ca^{2+} transients at negative voltages followed by up to fivefold larger skeletal-type transients at positive voltages. This indicates that nonskeletal channels only partially activate the Ca^{2+} release capacity of dysgenic myotubes.

Interestingly, the cause of this differential ability to activate Ca^{2+} release is not, as one might think, the difference between skeletal and cardiac-type activation of Ca^{2+} release. GFP-CSk53, a cardiac-based channel chimera with skeletal EC-coupling properties (Nakai et al., 1998), also induced small transients like those of GFP- α_{1C} and GFP- α_{1D} . Apparently channel isoforms and chimeras other than α_{1S} activate SR Ca^{2+} release less efficiently than the native channel, and transferring skeletal EC-coupling properties onto a cardiac-type channel is not sufficient to overcome this deficiency. It may well be that other properties specific to the skeletal α_{1S} subunit enable α_{1S} to activate more Ca^{2+} release channels or the same number more efficiently than non-skeletal channels. Thus, the body of the channel—skeletal or nonskeletal—as well as the region in the II-III loop important for skeletal-type activation of EC-coupling seems to be important for the magnitude of Ca^{2+} release achieved in reconstituted dysgenic myotubes.

The combined evidence from this and previous studies allows drafting of the following model of the role of CICR in skeletal muscle contraction. CICR appears to be a significant component of skeletal muscle EC-coupling (O'Brien et al., 2002). To activate CICR in skeletal muscle, a threshold concentration of Ca^{2+} in the triads needs to be exceeded. During the brief depolarization of an action potential, this is achieved only by channels located in close range of the RyRs within the triad junction, but not by Ca^{2+} influx outside the triads. Interestingly, Ca^{2+} currents the size of the skeletal α_{1S} are capable of activating CICR, whereas SR Ca^{2+} release through the RyRs alone cannot sustain its own further release after repolarization. Thus, in normal EC-coupling CICR is not regenerative but amplifies the trigger Ca^{2+} signal while remaining under the strict control of the voltage-activated channels. Upon long depolarization, and possibly also during tetanic stimulation or certain pathologic conditions like malignant hyperthermia, the strict local control of CICR breaks down and regenerative activation of CICR in skeletal muscle may occur. Thus, the spatial arrangement of voltage-activated channels and SR Ca^{2+} release channels in the triad plays an essential part in the control of Ca^{2+} release in skeletal muscle EC-coupling.

We thank Drs. P. Lory and S.J. Dubel (Institut de Genetique Humaine, CNRS UPR 1142, Montpellier) for generously supplying the expression plasmid for GFP- α_{1G} , Dr. W. Melzer and his team in Ulm for fruitful exchange of know-how, Dr. J. Hoflacher and Ms. D. Kandler for their experimental help, and Dr. H. Glossmann for generously providing support for the pursuit of this project.

This work was supported in part by the European Commissions Training and Mobility of Researchers Network Grant ERBFMRXCT960032 (to B.E.F.) and by the Fonds zur Förderung der wissenschaftlichen Forschung, Austria, Grants P12653-MED and P15338-MED (to B.E.F.), and P13831-GEN and Austrian National Bank (to M.G.). This work is part of the Ph.D. thesis of N.K.

REFERENCES

- Adams, B. A., T. Tanabe, A. Mikami, S. Numa, and K. G. Beam. 1990. Intramembrane charge movement restored in dysgenic skeletal muscle by injection of dihydropyridine receptor cDNAs. *Nature*. 346:569–572.
- Adams, B. A., Y. Mori, M. S. Kim, T. Tanabe, and K. G. Beam. 1994. Heterologous expression of BI Ca^{2+} channels in dysgenic skeletal muscle. *J. Gen. Physiol.* 104:985–996.
- Baylor, S. M., W. K. Chandler, and M. W. Marshall. 1983. Sarcoplasmic reticulum calcium release in frog skeletal muscle fibres estimated from Arsenazo III calcium transients. *J. Physiol.* 344:625–666.
- Bers, D. M. 2000. Calcium fluxes involved in control of cardiac myocyte contraction. *Circ. Res.* 87:275–281.
- Beurg, M., M. Sukhareva, C. Strube, P. A. Powers, R. G. Gregg, and R. Coronado. 1997. Recovery of Ca^{2+} current, charge movements, and Ca^{2+} transients in myotubes deficient in dihydropyridine receptor beta 1 subunit transfected with beta 1 cDNA. *Biophys. J.* 73:807–818.
- Brum, G., E. Stefani, and E. Rios. 1987. Simultaneous measurements of Ca^{2+} currents and intracellular Ca^{2+} concentrations in single skeletal muscle fibers of the frog. *Can. J. Physiol. Pharmacol.* 65:681–685.
- Cannell, M. B., J. R. Berlin, and W. J. Lederer. 1987. Effect of membrane potential changes on the calcium transient in single rat cardiac muscle cells. *Science*. 238:1419–1423.
- Dietze, B., F. Bertocchini, V. Barone, A. Struk, V. Sorrentino, and W. Melzer. 1998. Voltage-controlled Ca^{2+} release in normal and ryanodine receptor type 3 (RyR3)-deficient mouse myotubes. *J. Physiol.* 513:3–9.
- Feldmeyer, D., W. Melzer, B. Pohl, and P. Zollner. 1990. Fast gating kinetics of the slow Ca^{2+} current in cut skeletal muscle fibres of the frog. *J. Physiol.* 425:347–367.
- Flucher, B. E., S. B. Andrews, S. Fleischer, A. R. Marks, A. Caswell, and J. A. Powell. 1993. Triad formation: organization and function of the sarcoplasmic reticulum calcium release channel and triadin in normal and dysgenic muscle in vitro. *J. Cell Biol.* 123:1161–1174.
- Flucher, B. E., S. B. Andrews, and M. P. Daniels. 1994. Molecular organization of transverse tubule/sarcoplasmic reticulum junctions during development of excitation-contraction coupling in skeletal muscle. *Mol. Biol. Cell.* 5:1105–1118.
- Flucher, B. E., N. Kasielke, and M. Grabner. 2000. The triad targeting signal of the skeletal muscle calcium channel is localized in the COOH terminus of the α_{1S} subunit. *J. Cell Biol.* 151:467–478.
- Garcia, J., M. Amador, and E. Stefani. 1989. Relationship between myoplasmic calcium transients and calcium currents in frog skeletal muscle. *J. Gen. Physiol.* 94:973–986.
- Garcia, J., and K. G. Beam. 1994. Calcium transients associated with the T type calcium current in myotubes. *J. Gen. Physiol.* 104:1113–1128.
- Garcia, J., T. Tanabe, and K. G. Beam. 1994. Relationship of calcium transients to calcium currents and charge movements in myotubes expressing skeletal and cardiac dihydropyridine receptors. *J. Gen. Physiol.* 103:125–147.
- Giannini, G., A. Conti, S. Mammarella, M. Scrobogna, and V. Sorrentino. 1995. The ryanodine receptor/calcium channel genes are widely and

- differentially expressed in murine brain and peripheral tissues. *J. Cell Biol.* 128:893–904.
- Grabner, M., R. T. Dirksen, and K. G. Beam. 1998. Tagging with green fluorescent protein reveals a distinct subcellular distribution of L-type and non-L-type Ca^{2+} channels expressed in dysgenic myotubes. *Proc. Natl. Acad. Sci. USA.* 95:1903–1908.
- Grabner, M., R. T. Dirksen, N. Suda, and K. G. Beam. 1999. The II–III loop of the skeletal muscle dihydropyridine receptor is responsible for the bidirectional coupling with the ryanodine receptor. *J. Biol. Chem.* 274:21913–21919.
- Hell, J. W., R. E. Westenbroek, C. Warner, M. K. Ahljianian, W. Prystay, M. M. Gilbert, T. P. Snutch, and W. A. Catterall. 1993. Identification and differential subcellular localization of the neuronal class C and class D L-type calcium channel $\alpha 1$ subunits. *J. Cell Biol.* 123:949–962.
- Iwashima, Y., W. Pugh, A. M. Depaoli, J. Takeda, S. Seino, G. I. Bell, and K. S. Polonsky. 1993. Expression of calcium channel mRNAs in rat pancreatic islets and downregulation after glucose infusion. *Diabetes.* 42:948–955.
- Jurkat-Rott, K., U. Uetz, U. Pika-Hartlaub, J. Powell, B. Fontaine, W. Melzer, and F. Lehmann-Horn. 1998. Calcium currents and transients of native and heterologously expressed mutant skeletal muscle DHP receptor α subunits (R528H). *FEBS Lett.* 423:198–204.
- Kollmar, R., L. G. Montgomery, J. Fak, L. J. Henry, and A. J. Hudspeth. 1997. Predominance of the $\alpha 1D$ subunit in L-type voltage-gated Ca^{2+} channels of hair cells in the chicken's cochlea. *Proc. Natl. Acad. Sci. USA.* 94:14883–14888.
- Koschak, A., D. Reimer, I. Huber, M. Grabner, H. Glossmann, J. Engel, and J. Striessnig. 2001. $\alpha 1D$ (Cav1.3) subunits can form L-type Ca^{2+} channels activating at negative voltages. *J. Biol. Chem.* 276:22100–22106.
- Lipp, P., M. Egger, and E. Niggli. 2002. Spatial characteristics of sarcoplasmic reticulum Ca^{2+} release events triggered by L-type Ca^{2+} current and Na^+ current in guinea-pig cardiac myocytes. *J. Physiol.* 542:383–393.
- Melzer, W., E. Rios, and M. F. Schneider. 1984. Time course of calcium release and removal in skeletal muscle fibers. *Biophys. J.* 45:637–641.
- Monteil, A., J. Chemin, E. Bourinet, G. Mennessier, P. Lory, and J. Nargeot. 2000. Molecular and functional properties of the human $\alpha 1G$ subunit that forms T-type calcium channels. *J. Biol. Chem.* 275:6090–6100.
- Nagasaki, K., and M. Kasai. 1983. Fast release of calcium from sarcoplasmic reticulum vesicles monitored by chlortetracycline fluorescence. *J. Biochem. (Tokyo).* 94:1101–1109.
- Nakai, J., T. Tanabe, T. Konno, B. Adams, and K. G. Beam. 1998. Localization in the II–III loop of the dihydropyridine receptor of a sequence critical for excitation-contraction coupling. *J. Biol. Chem.* 273:24983–24986.
- O'Brien, J. J., W. Feng, P. D. Allen, S. R. Chen, I. N. Pessah, and K. G. Beam. 2002. Ca^{2+} activation of RyR1 is not necessary for the initiation of skeletal-type excitation-contraction coupling. *Biophys. J.* 82:2428–2435.
- Powell, J. A., L. Petherbridge, and B. E. Flucher. 1996. Formation of triads without the dihydropyridine receptor α subunits in cell lines from dysgenic skeletal muscle. *J. Cell Biol.* 134:375–387.
- Rios, E., and M. D. Stern. 1997. Calcium in close quarters: microdomain feedback in excitation-contraction coupling and other cell biological phenomena. *Annu. Rev. Biophys. Biomol. Struct.* 26:47–82.
- Smith, J. S., R. Coronado, and G. Meissner. 1986. Single channel measurements of the calcium release channel from skeletal muscle sarcoplasmic reticulum. Activation by Ca^{2+} and ATP and modulation by Mg^{2+} . *J. Gen. Physiol.* 88:573–588.
- Stern, M. D., L. S. Song, H. Cheng, J. S. Sham, H. T. Yang, K. R. Boheler, and E. Rios. 1999. Local control models of cardiac excitation-contraction coupling. A possible role for allosteric interactions between ryanodine receptors. *J. Gen. Physiol.* 113:469–489.
- Takimoto, K., D. Li, J. M. Nerbonne, and E. S. Levitan. 1997. Distribution, splicing and glucocorticoid-induced expression of cardiac $\alpha 1C$ and $\alpha 1D$ voltage-gated Ca^{2+} channel mRNAs. *J. Mol. Cell. Cardiol.* 29:3035–3042.
- Tanabe, T., K. G. Beam, J. A. Powell, and S. Numa. 1988. Restoration of excitation-contraction coupling and slow calcium current in dysgenic muscle by dihydropyridine receptor complementary DNA. *Nature.* 336:134–139.
- Tanabe, T., A. Mikami, S. Numa, and K. G. Beam. 1990. Cardiac-type excitation-contraction coupling in dysgenic skeletal muscle injected with cardiac dihydropyridine receptor cDNA. *Nature.* 344:451–453.
- Wilkens, C. M., N. Kasielke, B. E. Flucher, K. G. Beam, and M. Grabner. 2001. Excitation-contraction coupling is unaffected by drastic alteration of the sequence surrounding residues L720–L764 of the $\alpha 1S$ II–III loop. *Proc. Natl. Acad. Sci. USA.* 98:5892–5897.
- Xu, L., A. Tripathy, D. A. Pasek, and G. Meissner. 1999. Ruthenium red modifies the cardiac and skeletal muscle Ca^{2+} release channels (ryanodine receptors) by multiple mechanisms. *J. Biol. Chem.* 274:32680–32691.
- Zidanic, M., and P. A. Fuchs. 1995. Kinetic analysis of barium currents in chick cochlear hair cells. *Biophys. J.* 68:1323–1336.